QUARTERLY PROGRESS REPORT NO. 4

CONTRACT NASW-1035

RESEARCH ON GRAVITATIONAL MASS SENSORS

15 JULY through 14 OCTOBER 1965

HUGHES

HUGHES AIRCRAFT COMPANY

HUGHES RESEARCH LABORATORIES • MALIBU

HUGHES RESEARCH LABORATORIES
Malibu, California

a division of hughes aircraft company

RESEARCH ON GRAVITATIONAL MASS SENSORS

Quarterly Progress Report No. 4
Contract No. NASW-1035
15 July 1965 through 14 October 1965

Robert L. Forward, Principal Investigator
Curtis C. Bell, J. Roger Morris and
John M. Richardson, Contributors

TABLE OF CONTENTS

LIST OF ILLUSTRATIONS

I. INTRODUCTION AND SUMMARY

A. Purpose and Technical Objectives

The ultimate objective of our work on gravitational mass sensors is the development of a small, lightweight, rugged sensor to be used on lunar orbiters to measure the mass distribution of the moon and on deep space probes to measure the mass of the asteroids. The basic concepts, the theoretical limitations, and the possible applications have been investigated and are discussed in Section II of Quarterly Progress Report No. 1.

The purpose of the present research program is

1. To develop and refine experimental techniques for the measurement of gravitational and inertial fields using rotating elastic systems.

2. To develop a more complete understanding of these types of sensors so that accurate predictions of sensor behavior can be made with are based on practical system configurations and measured device sensitivity.

B. Summary of Problem Areas

The major problem area can be summarized in one word — noise. This noise includes background clutter due to external forces and masses other than the one under investigation, external electrical noise and mechanical vibrations, and internal thermal and electronic noise in the sensor and amplifiers. The force of gravitational attraction is very weak, even for large masses, and every effort must be made in sensor design and operation to develop and utilize discrimination techniques that will allow the weak gravitational signal to be picked out from the background clutter and noise.

The problems of background clutter are nearly independent of the particular sensor design. It is felt that the techniques discussed in Section II-D-2 of Quarterly Progress Report No. 1, Background Rejection, will suffice for elimination of this source of noise.

The problems of externally and internally generated electrical and mechanical noise have been overcome in previous work on non-rotating gravitational sensors and the experience gained during this work will aid in the investigation of the very similar problems in rotating sensors. It is expected that each sensor design will have its own

versions of these problems and that a major portion of the experimental work will be spent in locating and eliminating or discriminating against these sources of extraneous noise.

One minor problem area which will require special attention in the theoretical portion of the program is the instability and cross-coupling effects that are common to mechanically rotated systems. Typical examples are given in the Appendix of Quarterly Progress Report No. 1 and Section III of this report. These problems can be avoided by proper choice of sensor configuration and sensor operation based on a thorough theoretical analysis and preliminary experimental studies of each proposed design before extensive experimental work is done.

C. Summary of General Approach

The program has started with parallel efforts consisting of detailed theoretical study and preliminary experimental work. The various possible sensor configurations are being investigated theoretically to determine their suitability as mass sensors under the assumed operating conditions. Various combinations of promising sensor designs and sensor support and drive mechanisms are being constructed and operated to verify qualitatively the sensor characteristics, develop signal readout techniques, and search for unexpected sources of instabilities and noise. No attempt will be made to look for gravitational interactions at this stage.

After the preliminary work, one of the sensor configurations will be chosen as the basis for a feasibility model, and a carefully designed version will be constructed. The remainder of the program will be expended in studying the feasibility model both experimentally and theoretically, locating and eliminating the sources of extraneous noise, and determining the sensitivity to gravitational fields. The program objective is a sensor that will detect the presence of a small, nearby moving mass through gravitational interactions.

D. Summary of Work to Date

This work began when the completed contract was received on 26 October 1964. The original study by R. L. Forward on the gravitational mass sensor was analyzed by C. C. Bell in a more general manner. (See Appendix of Quarterly Progress Report No. 1.) This analysis indicates that radially vibrating sensor structures generally are incapable of measuring the gravitational force gradient because the sensor will fly apart at the necessary rotation speeds.

The most promising form of gravitational mass sensor has been found to be a cruciform shaped spring-mass system. A number of different cruciform sensor heads (see Fig. 20 in Section II-D, and Fig. 6 in the Appendix, of Quarterly Progress Report No. 2) have been designed and studied experimentally. They all have demonstrated a basic structural stability under high rotation speed. A continuing theoretical study of the transversely vibrating cruciform sensor structure has been under way. The model used for the analysis consists of a central mass, four equal sensing masses on transversely vibrating arms, and a sensed mass. The analysis is quite complicated because of the multiplicity of masses and springs, the nonuniform character of the gravitational field, and the requirement that the restoring forces in the sensor include the centrifugal force and the coupling between the arms as well as the spring constant of the arms. The results of these analyses indicate that there is a particular mode of vibration of the sensor — the tuning fork mode (see Fig. 12(a) in this report) — that is at a different frequency then the other modes, responds to the presence of a gravitational force gradient field when rotated at half of its vibrational frequency, and yet does not respond to inertial forces.

The readout of the very small (10^{-10} in.) vibrations in the sensor arms is accomplished by the use of piezoelectric strain transducers attached to the sensor arms at the point of maximum strain. These transducers have a voltage-strain characteristic of 10^5 V/unit strain and have been used in previous work to measure motions down to 10^{-13} in. The voltage output expected of such a sensor due to the gravitational force gradient of a mass M at a distance R is:

$$V = \frac{3GM\ Q\ 3cr}{2R^3(2\omega)^2L^2}\ \sigma \sin 2\omega t \approx \frac{3GM\ \tau\ 3cr}{2R^3(2\omega)L^2}\ \sigma \sin 2\omega t \qquad (1)$$

where

$Q \equiv$ quality factor of the sensor resonance

$GM/R^3 \equiv$ gravitational gradient

$\omega \equiv$ angular frequency of rotation of the sensor

$\tau \equiv$ integration time $\approx \frac{Q}{2\omega}$

$r \equiv$ radial distance of sensor end mass from center of sensor rotation

$L \equiv$ length of sensor arm

$c \equiv$ half thickness of sensor arm

$\sigma \equiv$ transducer factor of strain transducer ($\sim 10^5$ V/in./in.).

If we assume a gravitational gradient due to the earth, the voltage output from the present monolithic sensors with a Q of 100 and a resonant frequency of 115 Hz is greater than 4 μV. The newer designs with a lower frequency of operation and a better geometry factor should have voltage outputs greater than 13 μV. These voltages are easily measured with standard laboratory equipment.

The results of various design studies and experimental investigations indicate that our present strain transducers, amplifiers, and other electronic components are more than adequate for the problem of seeing the gravitational gradient signals.

One of the problems which has arisen in our study of cruciform sensors is that of maintaining adequate frequency separation between the gravitational gradient sensing mode of the sensor and the other possible modes of vibration of the sensor and the sensor mounting structure. If the sensor head is held too firmly by the sensor mount, the sensor vibrational modes all converge to the same frequency. If the sensor is held too loosely, the sensor mount cannot resist the centrifugal force when the sensor is rotated. When the sensor is rotating, the modes tend to shift in frequency in a complicated, but predictable, manner. This often brings the gradient sensing mode frequency close to one of the other mode frequencies, making it difficult to utilize frequency filtering techniques to separate out the gravitational gradient signals. However, the results of the combined theoretical and experimental program on the behavior of the sensor modes under rotation indicates that by proper design of the sensor and sensor mount, it is possible to operate the sensor at the desired rotation speed of one-half of the gradient sensing mode frequency and still maintain adequate frequency separation.

Since the sensors must be rotated in order to work, the major problem being studied is that of bearing noise. A number of different bearings have been fabricated for our purposes and their noise characteristics investigated.

A ball bearing mount using gyro bearings and a carefully balanced sensor was constructed first. (See Section III of Quarterly Progress Report No. 1.) This type of bearing proved, as expected, to be much too noisy for use with these sensors.

An air bearing support and drive was then constructed by the Hughes Aerospace Group. The structure consists of a table supported both vertically and horizontally by an air bearing formed between a rotor tube and a channeled stator. The rotor tube also has a magnetic hysteresis ring which is driven by a synchronous motor stator constructed around the outside (see Section II-C of Quarterly Progress Report No. 2). The sensor chamber is then mounted on top of the rotor table and the voltages from the sensor are removed through the slip rings on the top.

A single-axis magnetic bearing support and drive was fabricated by the University of Virginia (see Section II-B of Quarterly Progress Report No. 3). In general, the unit performs well and is quite satisfactory for this program. The levitation circuits are slightly tricky in adjustment, but have proved to be capable of stably levitating the 6 lb mass of the sensor chamber and the iron pole cap. The compliance of the magnetic "spring" is very low so that there is good vibration isolation at the sensor frequency. When the servo loop is properly adjusted, the vertical stability of the support is good, except for a long term drift which requires that the servo gain be adjusted periodically. The pancake motor drive works quite well, although the available torque is necessarily limited by the relatively large air gaps that result from the levitation requirements.

Noise tests were conducted on these bearings using a sensor on a torsion wire mount inside a vacuum chamber. Readout was accomplished by means of slip rings running directly into a General Radio tuned preamplifier having an equivalent input noise of 0.050 μV. The first tests were undertaken to discover the sources of noise in the bearings under nonrotating operation. When the sensor chamber was suspended from a rubber band, the noise output was essentially flat with an amplitude of about 0.1 μV. When the sensor was sitting on the air bearing with no air flowing through the bearing, the noise output was essentially flat with an amplitude of about 0.2 μV. The increase in noise output resulted from the vibrations in the workbench. When the air pressure was turned on, levitating the sensor, the noise increased considerably. The background level was then 0.6 μV with a peak at the translational mode (220 Hz) of 10 μV, and a peak at the gradient sensing mode (170 Hz) of 1.5 μV. Several air bearing rotors with various gaps were tested with the result that the noise seemed to be linearly proportional to the amount of air flow. When the iron pole cap was attached to the sensor chamber and suspended in the magnetic bearing, the background noise level was about 0.15 μV.

Bearing noise tests were then made under dynamic conditions. The first tests were made by bringing the sensor up to speed, turning the drive off, and measuring the noise output as the sensor coasted down. It was found, in general, that under dynamic as well as static tests, the air bearing is 14 dB or more noisier than the magnetic bearing. This excess noise seems to result from the rush of air through the bearing and there is no obvious way to eliminate the problem. These tests indicated that for our purposes, a magnetic support generally is superior to the air bearing support.

On the basis of these tests it was decided to utilize a magnetic bearing in the feasibility model. A three-axis magnetic bearing and drive was ordered from the Cambridge Thermionic Corp., (CAMBION) in Cambridge, Massachusetts. This unit will have a smaller size and weight than the present bearing, as well as tighter tolerances on drift, and can be oriented in any direction.

While the three-axis magnetic bearing is being fabricated, the single-axis bearing was reworked to improve its performance and an external vacuum chamber added to reduce air drag effects on the rotating sensor chamber. This unit was used for an extended series of vibrational mode tests, sensor mount studies, and bearing noise tests.

When noise tests were made with the magnetic support motor drive on, two additional noise sources due to the drive fields were found. One was a general noise level increase due to hash and hum in the drive amplifiers. This caused about 3 μV of noise and was seen only when the drive amplifiers were turned on; but the sensor was not yet rotating. This noise will be eliminated by filtering the output of the drive amplifiers. The second was a torquing noise resulting from the interaction of the rotating drive field and the remnant magnetic poles in the hysteresis plate. This noise is a direct function of the drive power and, for synchronous operation with large drive levels, can be many millivolts. However, if the drive is lowered to a level just sufficient to maintain synchronous rotation, the noise level drops to the level seen under free rotation conditions.

The latest set of noise measurements were taken on a sensor mounted on a 0.020 in. diameter torsion wire inside an evacuated sensor chamber. Although this sensor system was the best available at the time, it still had a vibration sensitive translational mode within a few hertz of the gradient sensing mode. Three tests were run; the first used regular slip ring brushes while the sensor chamber was run in air. The second test was the same as the first except that the external vacuum chamber was added and evacuated in order to cut down windage noise. The data show that the difference between air and vacuum for this configuration was very slight, indicating that windage is not yet a problem. However, the slip ring brushes were found to be responsible for the large noise peaks (200 mV) at the rotational speeds corresponding to the translational mode and the gradient sensing mode. In the third test, the standard slip ring brushes were replaced with special fine copper wire brushes with low mass and low mechanical coupling. The data taken with the light slip ring brush had a maximum noise peak of about 8 mV at 108 Hz when the sensor was rotating at the desired operating speed of 3240 rpm (54 rps). This measured noise level is quite high and should decrease substantially when better resolution between the various modes is obtained either by finding a configuration with better mode separation or by using narrower bandwidths in our amplifiers.

Since slip ring wobble seemed to be the major source of noise, the telemetry unit discussed in Section II-A of this report was constructed and operated with the same sensor in an effort to obtain comparative noise measurements, both with and without slip rings. However, the telemetry unit proved to be difficult to balance in the single-axis magnetic bearing and it has not been possible to obtain consistent measurements up to the time of this report.

A shortened version of Quarterly Progress Report No. 1 was submitted to the annual essay contest of the Gravity Research Foundation, New Boston, New Hampshire, as an essay entitled "Rotating Gravitational Sensors" by R. L. Forward, C. C. Bell, and J. R. Morris. The essay received fourth award.

A paper, "Mass Detection by Means of Measuring Gravity Gradients," by C. C. Bell, R. L. Forward, and J. R. Morris was prepared for the 2nd Annual AIAA Meeting and was given by Curtis Bell on 26 July 1965 in San Fracisco.

II. EXPERIMENTAL PROGRAM

A. Electronics Design Studies

The gravitational mass sensors being studied under this contract operate by sensing the gradient of the gravitational force produced by the mass. The presence of the gravitational gradients induces mechanical vibrations in the rotating sensor. The magnitude and phase of these vibrations indicate the strength and direction of the gravitational gradient.

In order for the vibrations to be conveniently observed, they must be converted into electrical signals, amplified, and removed from the rotating sensor. The method of transducing and removing the signals from the sensor has been reviewed this quarter and the results of these studies are presented below.

1. Strain Transducers

The vibrations of the sensor arms are converted to electrical signals by placing strain transducers on the arms. The units used have been Glennite SC-2 ceramic, piezoelectric transducers manufactured by Gulton Industries. These transducers have the advantages of small size (1/2 in. x 1/8 in. x 0.012 in.), high output ($\sim 10^5$ V/unit/strain) and high capacity (1000 pF). Their disadvantages are a somewhat variable output with temperature and humidity, and a mechanical Q low enough to reduce the Q of the sensor arm to which they are applied.

The following analysis of strain transducer behavior was conducted to determine how good our present transducers are in comparison to other possible configurations and materials.

The element used for analysis is a piece of piezoelectric material of Area A and thickness t strained in the direction shown below. The fundamental piezoelectric relationship is:

$$q = d S A \qquad (2)$$

D416-14

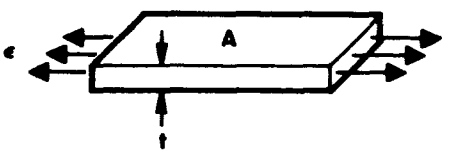

where q is the induced charge, d the piezoelectric constant, and S the stress on a plane perpendicular to A.

To this must be added the stress-strain relationship for the material

$$S = Y \epsilon \ , \tag{3}$$

where ϵ is the strain, and Y is Young's modulus.

The capacity-voltage-charge formula is

$$V = q/C \tag{4}$$

and the parallel plate capacity formula is

$$C = \kappa \varepsilon_o \frac{A}{t} \ , \tag{5}$$

where κ is the relative dielectric constant and ε_o is the capacitivity of free space.

The above relationships may be combined in several ways to relate voltage to strain.

$$\sigma = \frac{V}{\epsilon} = \frac{d\,Y\,A}{C} = \frac{d\,Y\,t}{\kappa\,\varepsilon_o} \tag{6}$$

In addition, four other factors must be considered in evaluating a transducer:

1. It must be thin enough to accurately measure the strain on the surface to which it is applied.

2. It should not seriously deteriorate the Q of the vibrating arm.

3. Its capacity should not be too low.

4. Its output should not vary with ambient conditions.

In Table I, four ceramic materials (made by Gulton) are compared with quartz and our present transducer. Each material is treated as though it were made into a transducer similar to the one now in use. An exception is made for quartz which is assumed to be one-tenth the thickness of the ceramic transducers. This can be done because quartz is easy to work with and such a thickness is quite practical.

The important conclusions to be drawn from the data shown in the table areas follows:

- There is no immediate advantage to be gained by having new strain transducers made as none of the materials show significant advantages over our present transducer at this stage of the project.

- If, in the future, higher output is desired, it may be obtained by using HST-41 or HDT-31 in a thicker transducer. Since output is proportional to thickness, the output could be increased by 10 without reducing the capacity below a practical level. The resulting transducer would be quite thick, however, and might cause a bonding and Q problem.

- If, in the future, we want better stability and Q, a quartz transducer could be made with roughly the same output we have now. Each transducer would have a very high output impedance, however, which would necessitate using several parallel transducers to bring the impedance down to practical levels. ($Z \cong 10\ M\Omega$ for 4 transducers at 100 cps).

2. Transmitter

The electrical signals from the strain transducers must be removed from the suspended and rotating sensor. Slip rings were used for our preliminary investigations, but they proved to have several disadvantages, the most serious of which were vibrational noise generation and general handling difficulties. In order to eliminate these, an amplifier-transmitter was designed and constructed (see Fig. 1). The The present schematic of this device is shown in Fig. 2.

TABLE I

Characteristics of Various Piezoelectric Materials

Material and Thickness t, mm	Piezoelectric Constant d, m/V	Young's Modulus Y, N/m^2	Dielectric Constant κ	Capacitance C pF	Strain-Voltage Ratio, V/unit strain
Present Ceramic (Glennite SC-2) 0.28	(No data available)			~1000	$\sim 1 \times 10^5$
Quartz 0.028	2.3×10^{-12}	8.6×10^{10}	4.6	41	1.4×10^5
HD 11 Ceramic 0.28	24×10^{-12}	14.2×10^{10}	600	530	1.7×10^5
HS 21 Ceramic 0.28	62×10^{-12}	11.5×10^{10}	1250	1100	2.0×10^5
HDT 31 Ceramic 0.28	120×10^{-12}	8×10^{10}	1300	1150	2.2×10^5
HST 41 Ceramic 0.28	140×10^{-12}	7.3×10^{10}	1800	1600	1.9×10^5

M 4289

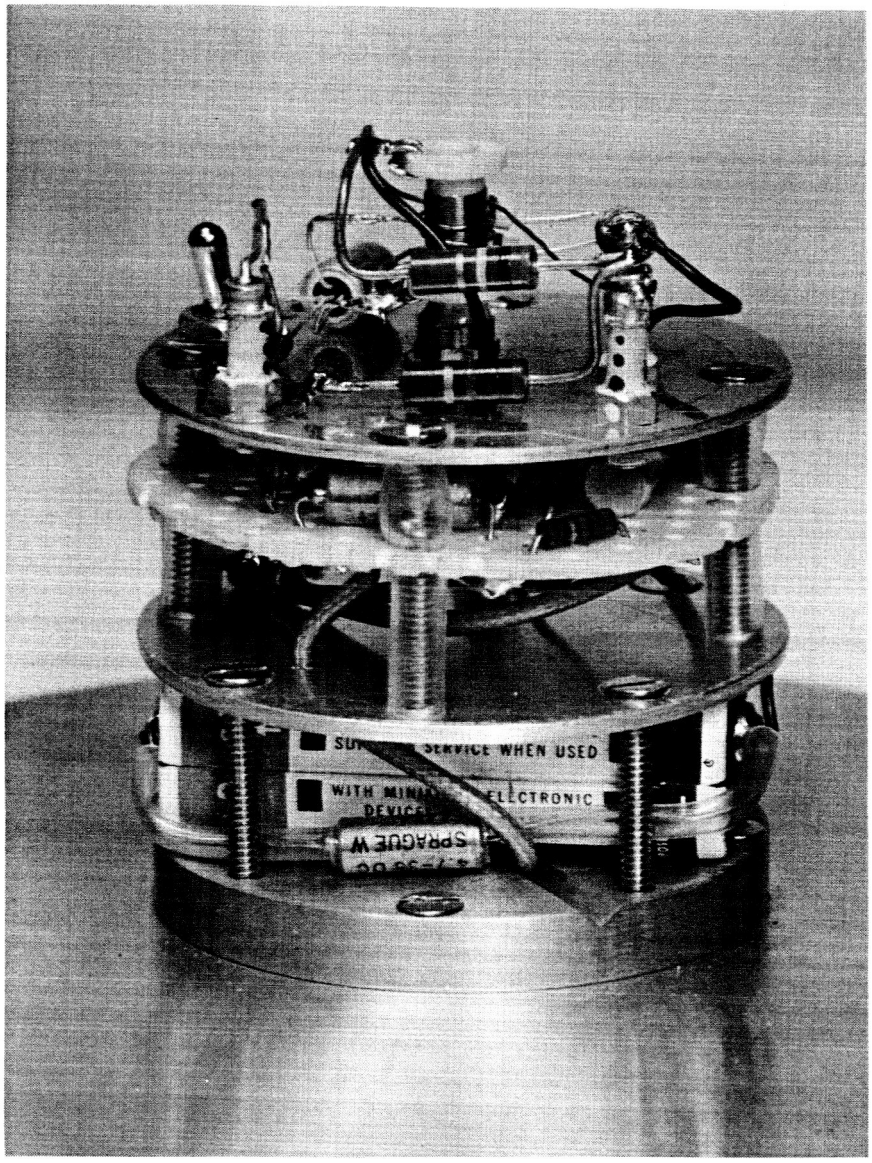

Fig. 1. Telemetering unit.

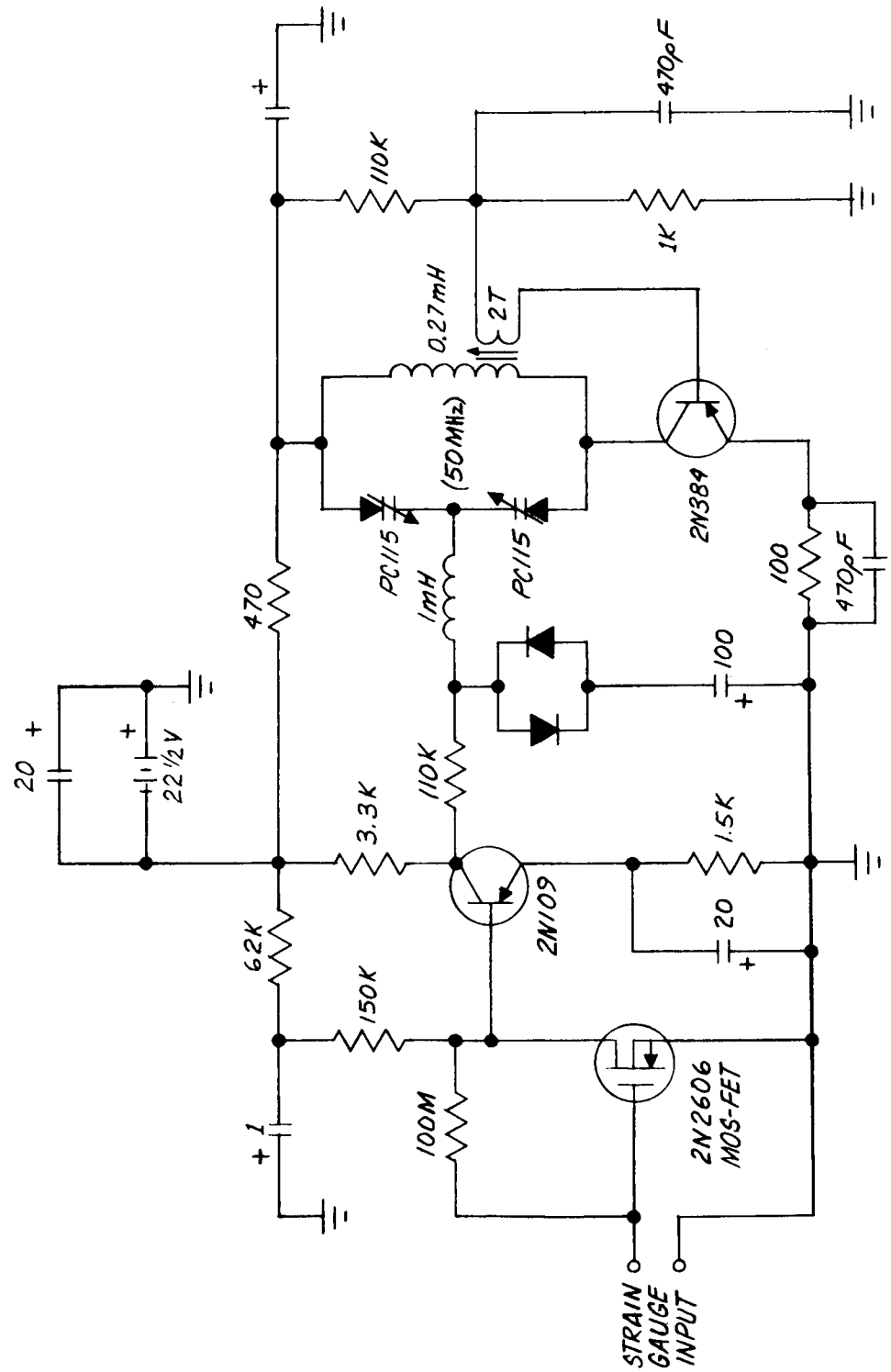

Fig. 2. Amplifier-transmitter schematic.

The first amplifier stage has an input impedance of 10 MΩ to accommodate the high output impedance of the strain transducers. The amplifier has a gain of about 100. The modulation voltage to the Varicaps is limited to ± 0.4 V so that the 50 MHz carrier is not over modulated.

A Hallicrafters SX62B receiver detects the transmitted signal and delivers it with an over-all gain of about 700 and a noise level of 32 μV. (2.8 μV in a 5% band at 100 Hz.) This telemetering system allows us to see signals down to about 3 μV from the strain transducers. If a better signal-to-noise ratio is desired, it can easily be attained by adding another stage of gain to the amplifier.

The amplifer-transmitter unit was tested by attaching it to a sensor chamber, grounding its input and rotating it in the magnetic suspension. The greatest noise output seen under these conditions was 7 μV at 60 Hz. The output at frequencies above this was free of peaks and about 10 dB lower when the sensor was rotating synchronously at 2000 rpm. Metal objects moved close to the unit did not affect its output provided the receiver was properly tuned.

All preliminary tests of the transmitter-receiver system indicate that outputs from the strain transducer above 3 μV should be detectable. This is more than adequate for our present noise tests and further improvement in signal-to-noise ratio can be made later as the sensor noise level decreases.

B. Vibrational Mode Tests

One of the problems which has arisen in our study of cruciform gravitational mass sensors is that of maintaining adequate frequency separation between the gravitational gradient sensing mode of the sensor and the other possible modes of vibration of the sensor and sensor mount. The most promising mounting structure at present consists of a double ended torsion wire. (See Fig. 4(b) in Quarterly Progress Report No. 2.)

In order to develop experience with the behavior of the various modes as a function of torsion wire diameter and rotation speed, a number of mode tests were run using torsion wire mounts of differing thicknesses. The vibrational modes were measured by driving one or more of the strain transducers with a constant amplitude signal of varying frequency while looking for the resonance peaks on the output of the other transducers. The graphs in Figs. 3 through 6 show the measured resonance frequencies of four different sensor-torsion wire configurations as a function of rotation speed.

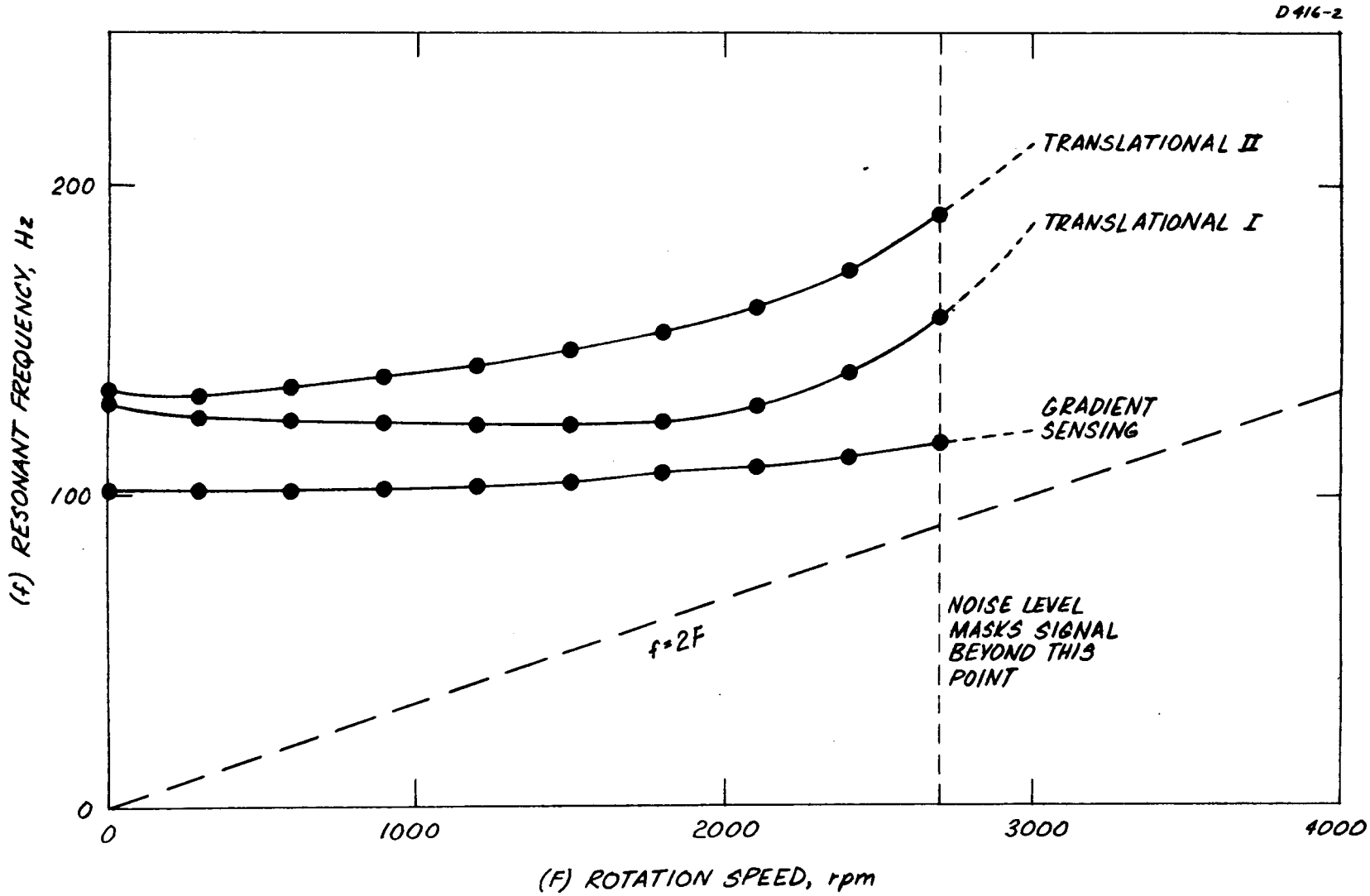

Fig. 3. Resonant modes of 100 Hz cruciform on 0.012 in. torsion wire.

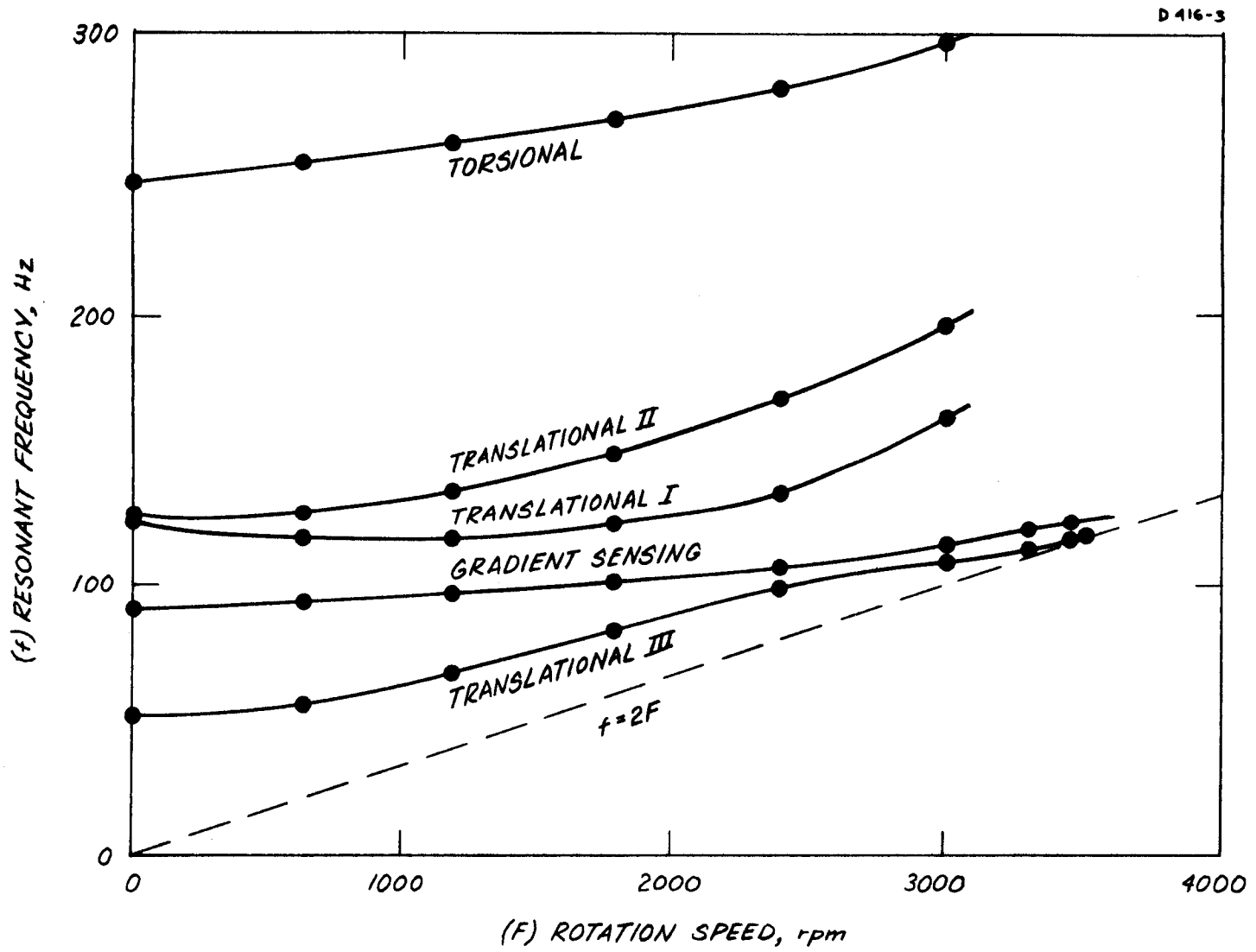

Fig. 4. Resonant modes of 90 Hz cruciform on 0.016 in. torsion wire.

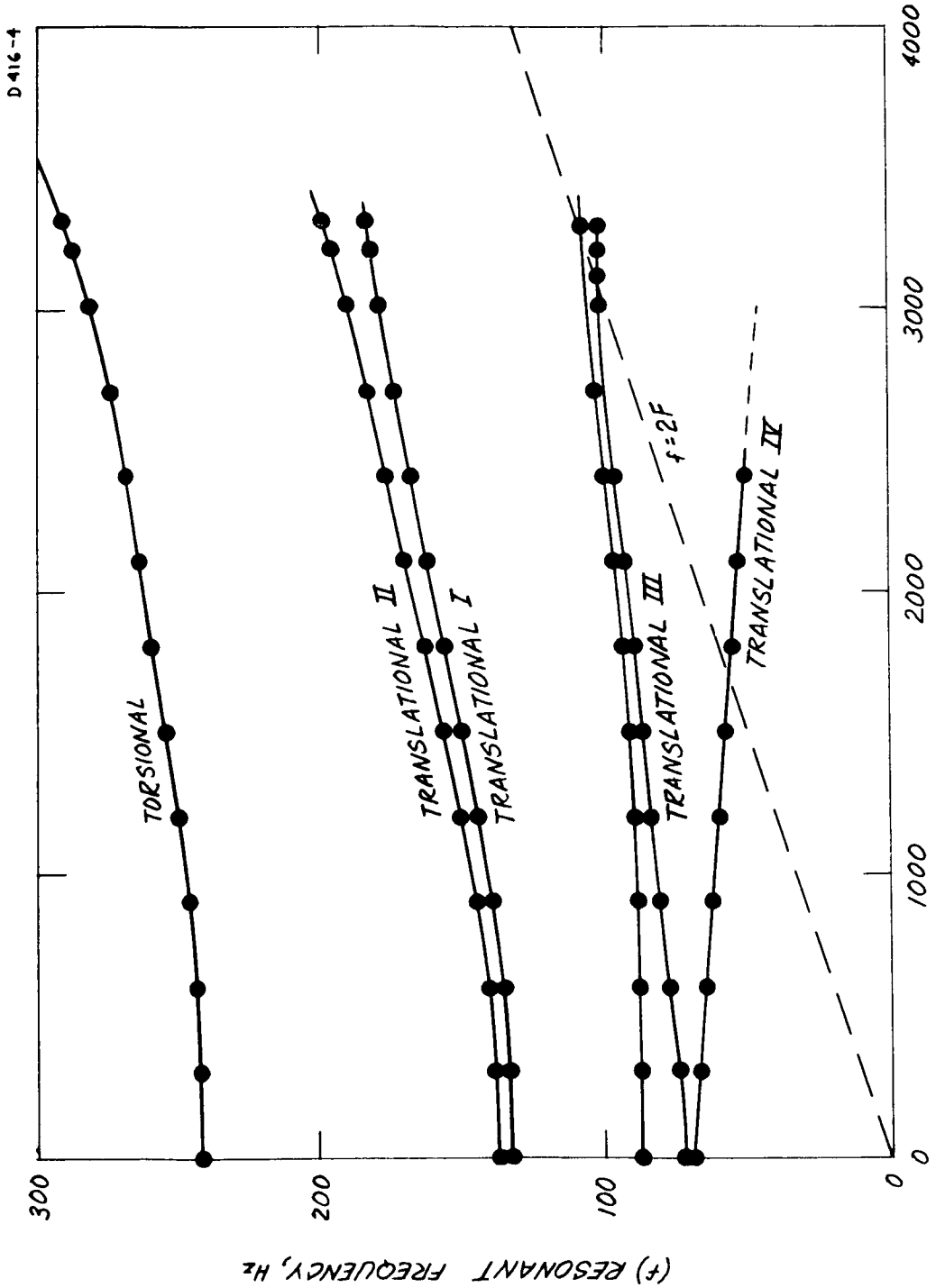

Fig. 5. Resonant modes of 90 Hz cruciform on 0.020 in. torsion wire.

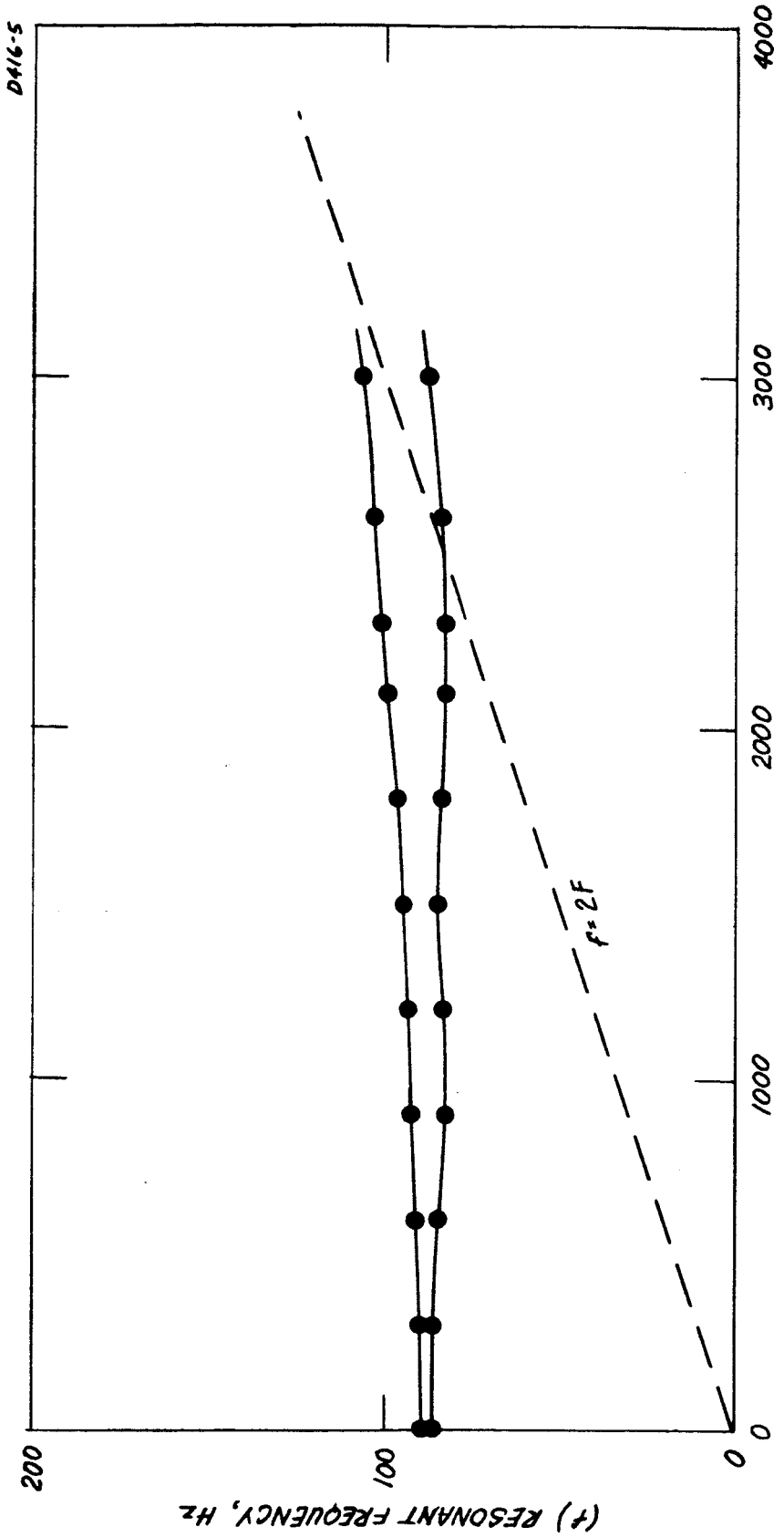

Fig. 6. Resonant modes of 90 Hz cruciform on 0.031 in. torsion wire.

The modes behave generally as predicted by the equations developed in Section III of this report. The sensor translational modes at 0 rpm are pushed up as the torsion wire becomes thicker, as predicted in Section III-A. The translational modes split and the gradient sensing mode frequency increases with increased rotation as predicted in Section III-B. This behavior is most apparent in Fig. 5 (0.020 in. diameter torsion wire) where all the modes were observed.

While testing the 0.012 and 0.016 in. torsion wires the sensor speed could not be brought above 2700 and 3000 rpm, respectively, because the signal from the electrically driven mode would be lost in the noise voltages generated by imbalances in the system. It was assumed that the smaller diameter torsion wires are too weak to withstand the centrifugal force and keep the sensor head from flying out from the center, causing a large imbalance.

In Fig. 5 (0.020 in. torsion wire) the sensor was able to attain the desired operating speed. The graph shows that both the tuning fork, or gradient sensing, mode and the downward shifted translational mode could be observed at these speeds. This configuration was used in the noise tests described in Section II-C of this report.

From the data in Fig. 5, it was felt that the desired mode separation might be attained at high speeds if thick torsion wire were used. Although the modes would be together at 0 rpm, they would perhaps split and separate from each other at higher speeds. Figure 6 shows that this is not the case. The two modes observed appear to be translational in nature, with no indication of a separate gradient sensing mode in between at any speed.

C. Comparative Noise Tests

A series of noise measurements were taken on a sensor mounted on a 0.020 in. diameter torsion wire inside an evacuated sensor chamber. Three tests were run, the first of which utilized regular slip ring brushes while the sensor chamber was run in air. The second test was the same as the first except that an external vacuum chamber was added and evacuated in an attempt to cut down windage noise. In the third test, the standard slip ring brushes were replaced with special fine copper wire brushes with low mass and low mechanical coupling. In each case the sensor chamber was brought up to speed and allowed to coast down. The data for these tests are reproduced in Fig. 7.

The data show that the difference between air and vacuum for this configuration is very slight, indicating that windage is not yet a problem. However, the slip ring brushes were found to be responsible for the large noise peaks at the rotational frequencies corresponding to the downward

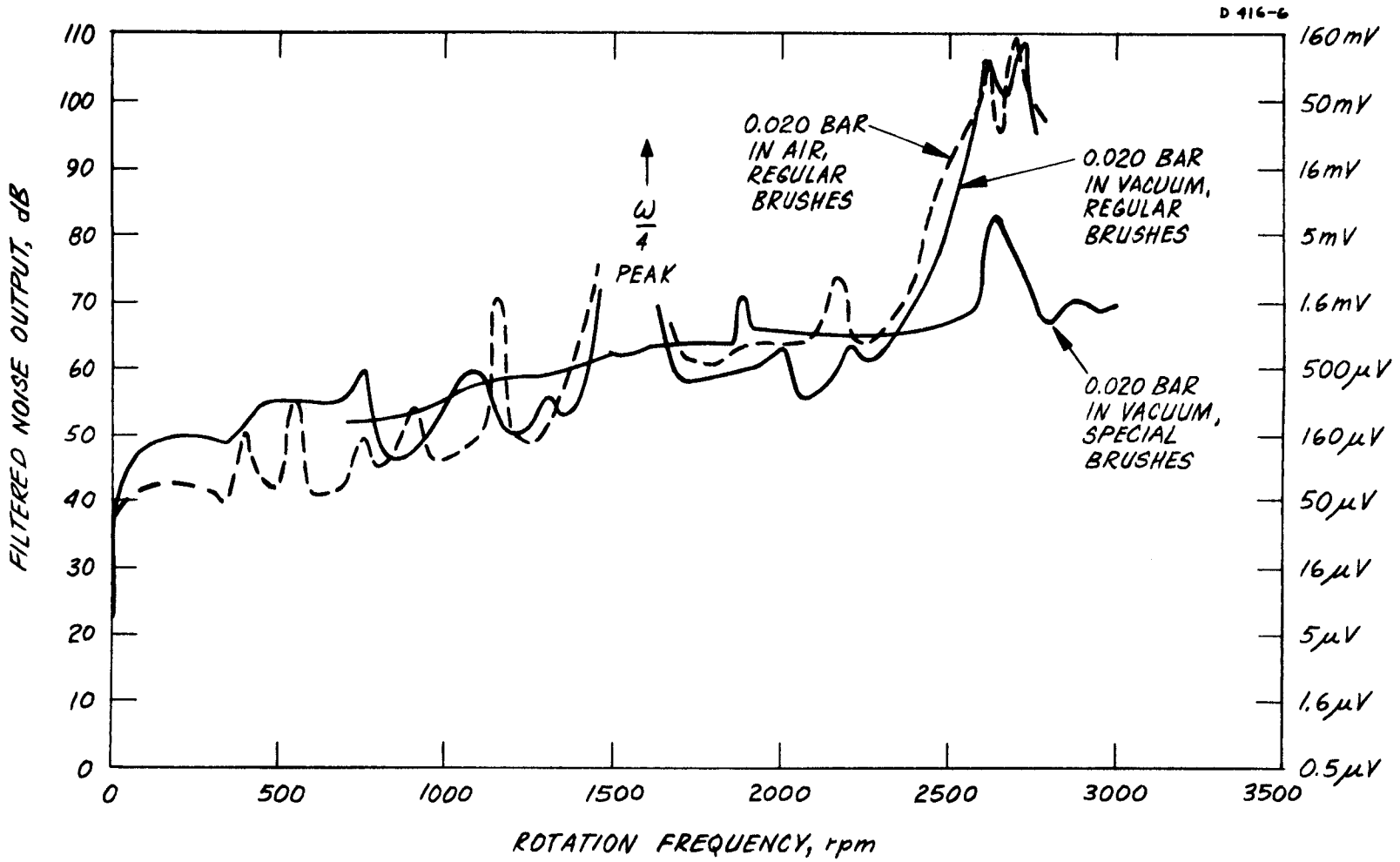

Fig. 7. Noise tests on 90 Hz cruciform on 0.020 in. torsion wire mount.

shifted translational mode and the gradient sensing mode. Even the low mass brushes appear to introduce some noise, but the level is about 30 dB lower and the curve is generally less erratic.

The data taken with the very light slip ring brush had a maximum noise peak of about 8 mV at 108 Hz when the sensor was rotating at the desired operating speed of 3240 rpm (54 rps).* This measured noise level is quite high; however, it should decrease substantially when better resolution between the various modes is obtained either by finding a configuration with better mode separation or by using narrower bandwidths in our amplifiers. (The tuned preamplifier used for these tests has a 5% bandwidth and only 26 dB rejection at subharmonics.)

If these data are compared with the noise data in Fig. 19 of Quarterly Progress Report No. 3, a discrepancy at low rotation speeds can be seen. The data in Fig. 19 is 20 to 30 dB lower near zero rpm, but has the same level as the present data above 1200 rpm (20 rps). The error is in the data in Quarterly Progress Report No. 3, and occurred because the raw data were not corrected upward to compensate for the impedance mismatch between the frequency sensitive strain transducers and the tuned preamplifiers at high gain settings. The data in this and future reports will be corrected for impedance mismatch.

Since slip ring wobble seemed to be the major source of noise, the telemetry unit discussed in Section II-A was constructed and operated with the same sensor in an effort to obtain comparative noise measurements, both with and without slip rings. However, the telemetry unit proved to be difficult to balance and it has not been possible to obtain consistent measurements up to the time of this report.

*Note added in proof: A recent test using a different sensor and sensor mount and a narrow bandwidth amplifier gave a maximum noise peak of 130 μV while operating synchronously at the desired operating speed. The gravitational gradient signals expected in our laboratory using this sensor are about 3% of this value or about 4 μV.

III. THEORETICAL PROGRAM

A major problem concerning cruciform gravitational mass sensors is in maintenance of adequate frequency separation between the various vibration sensitive resonant modes of the sensor system and the gradient sensing mode of the cruciform sensor head. If this frequency separation can be maintaned, it will then be possible to use narrow band amplifiers to separate the gravitationally driven sensor response from the inertially driven responses.

In earlier work, it was found that if the sensor has a small central mass and is well isolated from other masses by suspension from a weak spring, the gradient sensing mode is the lowest in frequency and is well separated from the rest of the vibrational modes (see Section II-B of Quarterly Progress Report No. 2.) However, as we have seen in Section II-B of this report, when rotation of the sensor is attempted while using a torsion wire mount with a weak spring constant, it is not possible to rotate the sensor up to the desired operating speed because the mount cannot resist the centrifugal forces. When the torsion wire mount stiffness is increased so that it can resist the centrifugal force, two new translational modes formed by the spring constant of the torsion wire and the total mass of the sensor become important. These modes cause the two translational modes in the sensor head to shift upward, helping to solve the mode separation problem. However, under rotation, the translational modes split, and at the desired rotational speed, become close enough to the gradient sensing mode to make frequency selection techniques difficult.

In an attempt to understand this behavior, some analyses of vibrational mode behavior were undertaken.

The first analysis studies the interference effects between the two translational modes formed by the spring constant of the torsion wire acting against the total sensor mass, and the two translational modes of the sensor head itself.

The second analysis studies the effect of rotation on the vibrational modes of the sensor alone. It is planned to add the torsional wire translational modes to this analysis in a future study in order to completely understand the interference effects of the two sets of translational modes and their variation with rotation speed.

A. Sensor Mount Resonance Analysis

In this analysis we wished to examine the interference or coupling effects between the translational modes of the sensor head and the translational modes of the sensor mounting structure. Although there

are two pairs of translational modes in the actual sensor, the x-polarized modes are identical to the y-polarized modes and it is sufficient to look only at one polarization.

The model that was assumed is illustrated in Fig. 8; it consists of two arms of mass m and spring constant K attached to a central mass. The central mass was assumed to have a mass 3m so that it would match the actual characteristics of our experimental models. The central mass is coupled to a large external mass through a torsion wire with spring constant K_o.

The model in Fig. 8 is mathematically analogous to the linear spring model shown in Fig. 9.

The equations of motion for this system are

$$3m\ddot{y} + K_o y + 2K(y - x) = 0 \qquad (7)$$

$$2m\ddot{x} + 2K(x - y) = F \quad . \qquad (8)$$

Using the Laplace transformation and solving, we obtain

$$x = \frac{F(3ms^2 + K_o + 2K)}{(3ms^2 + K_o + 2K)(2ms^2 + 2K) - 4K^2} \qquad (9)$$

$$y = \frac{2FK}{(3ms^2 + K_o + 2K)(2ms^2 + 2K) - 4K^2} \quad . \qquad (10)$$

These equations have poles when the denominator is zero

$$3m^2 s^4 + m(K_o + 5K)\, s^2 + K K_o = 0 \quad , \qquad (11)$$

or

$$s^2 = \frac{-(K_o + 5K) \pm (K_o^2 - 2 K K_o + 25 K^2)^{1/2}}{6m} \equiv -\omega^2 \qquad (12)$$

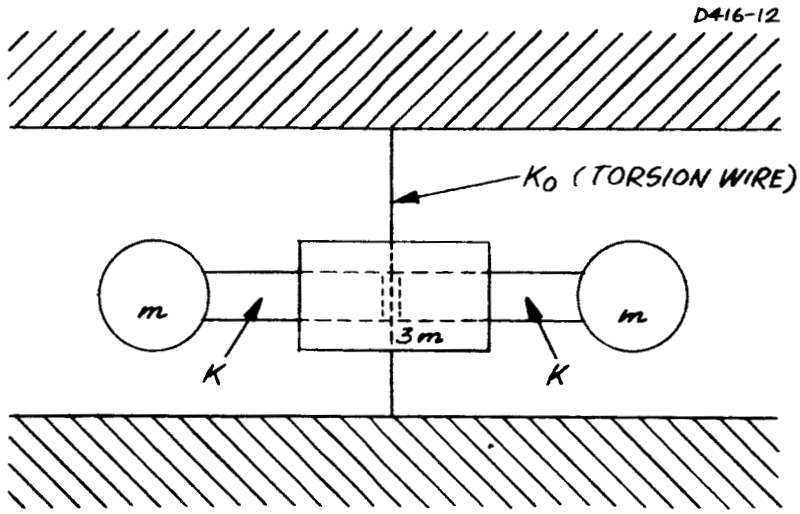

Fig. 8. Sensor-torsion wire model.

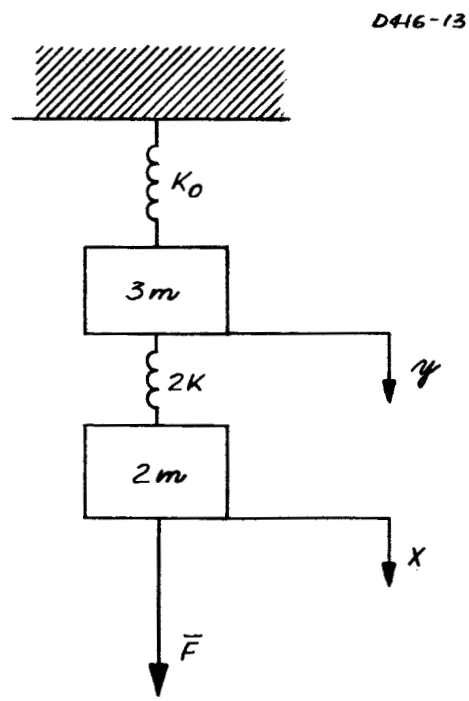

Fig. 9. Linear spring model.

where ω is the resonant mode frequency of the system. In order to make the results nondimensional, we will divide through by the resonance frequency $\sqrt{K/m}$ of a single isolated arm. (This is also the frequency of the gradient sensing mode.) This gives us the ratio of the various resonance frequencies as a function of the ratio of the spring constants.

$$\frac{\omega}{\sqrt{K/m}} = \left\{ \frac{K_o/K + 5 \pm \left[(K_o/K)^2 - 2K_o/K + 25 \right]^{1/2}}{6} \right\}^{1/2} . \tag{13}$$

When this equation is plotted for various values of spring constant ratios, we obtain Fig. 10.

Note that when the torsion wire spring is weak, its translational mode frequency is so low that it does not affect the translational mode of the sensor and the mode frequency is that of an isolated sensor (see Fig. 3 in Section II-B of this report). As the torsion wire frequency is raised, we note that the sensor translational mode frequency also rises as a result of an interference between the two modes. As the torsion wire frequency is raised even further, the sensor translational mode increases rapidly while the torsion wire translational mode approaches the gradient sensing mode frequency.

The optimum stiffness ratio for maximum frequency separation of both of the translational modes from the gradient sensing mode frequency at zero rotation speed seems to be approaximately $K_o/K = 3$.

To correlate this analysis with the experimental models we must calculate their spring constants. In the present sensor design, the arm stiffness is given by

$$K = \frac{EI}{L^3 \left[\frac{1}{3} + \frac{b}{L} + \left(\frac{b}{L} \right)^2 \right]} \tag{14}$$

where E, I, and L are the elastic modulus, section modulus, and length of the arm, respectively, and b is the effective radius of the end mass. (See Appendix of Quarterly Progress Report No. 3.) For the present geometry, the arm stiffness was calculated to be

$$K \cong 27 \text{ lb/in.} . \tag{15}$$

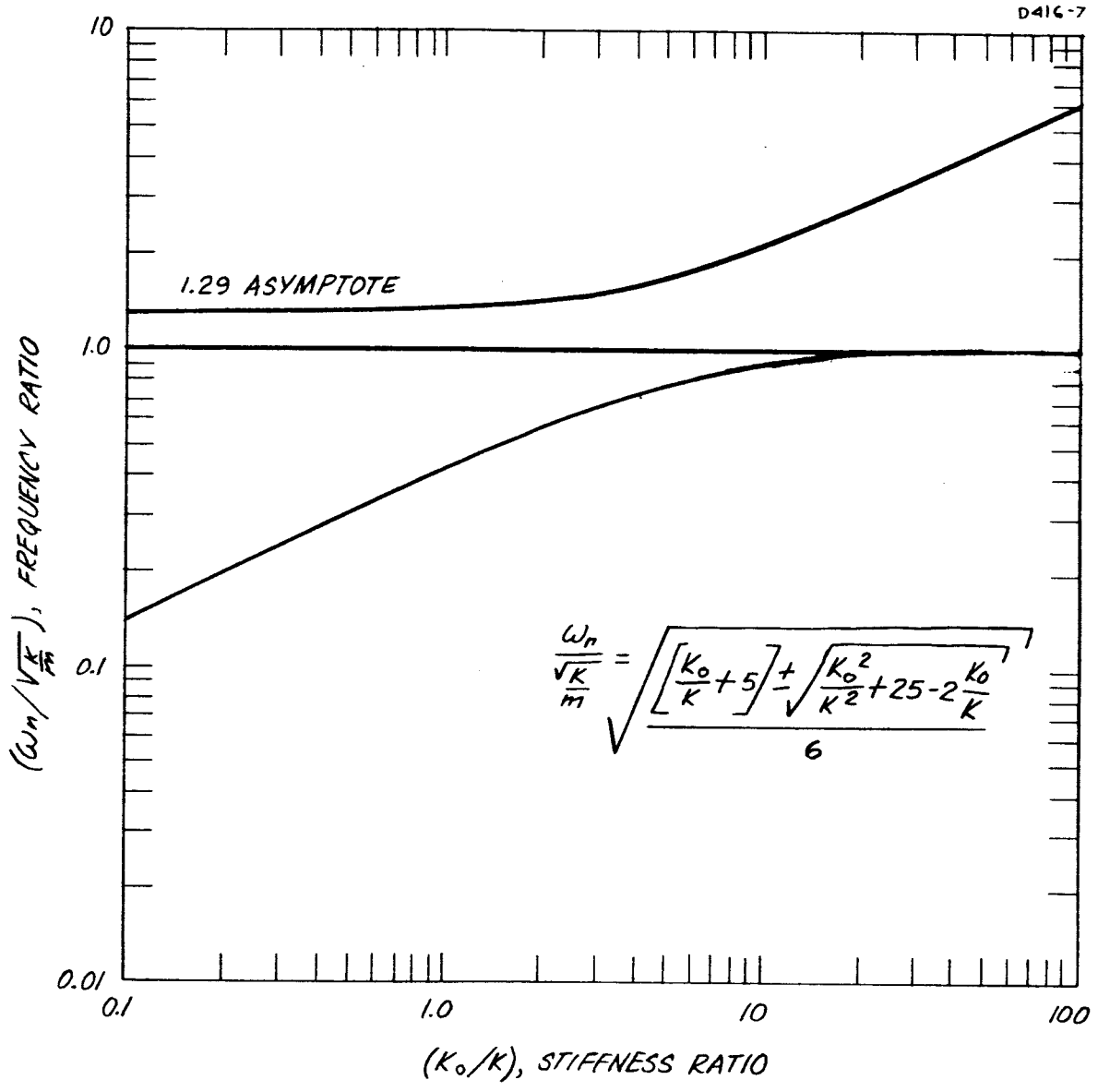

Fig. 10. Translational mode interference.

The torsion wire stiffness is given by

$$K_o = \frac{192\ EI}{L^3} = \frac{3\pi\ E\ D^4}{L^3} \qquad (16)$$

where E, D, and L are the elastic modulus, diameter, and length of the wire, respectively, and the section modulus $I = (\pi D^4)/64$. For the present geometry the torsion wire stiffness is

$$K_o = 1.31 \times 10^9\ D^4\ (\text{lb/in.}^5) \qquad (17)$$

and the ratio of the two stiffnesses as a function of the torsion wire diameter is given by

$$\frac{K_o}{K} = 4.8 \times 10^7\ D^4 \quad . \qquad (18)$$

This equation is plotted in Fig. 11. From this curve it can be seen that a diameter of 0.016 in. is necessary to obtain the optimum stiffness ratio of 3. A torsion wire mount of this diameter was fabricated; the results are shown in Fig. 4 of Section II-B. At zero rotation speed, we see that there are two sets of translational modes, one at 52 Hz and the other at 125 Hz. These are nearly equidistant from the gradient sensing mode at 90 Hz and thus we have obtained the desired maximum mode separation. Unfortunately, however, the translational modes were found to shift under rotation and the mode separation at the desired operating speed is much smaller than that at zero rotation speed.

B. Rotating Cruciform Mode Analysis

As a result of work in the earlier theoretical and experimental aspects of the contract, it has long been realized that the cruciform shaped gravitational mass sensors have four primary oscillation modes which involve the spring constant of the bending arms. These are the gradient sensing or tuning fork mode (Fig. 12(a)), a torsional mode (Fig. 12(b)) and two translational modes (Fig. 12(c)). In addition, there are higher order harmonics of these four basic modes as well as other modes of oscillation involving other elastic properties of the cruciform such as the torsional or longitudinal spring constants. These higher

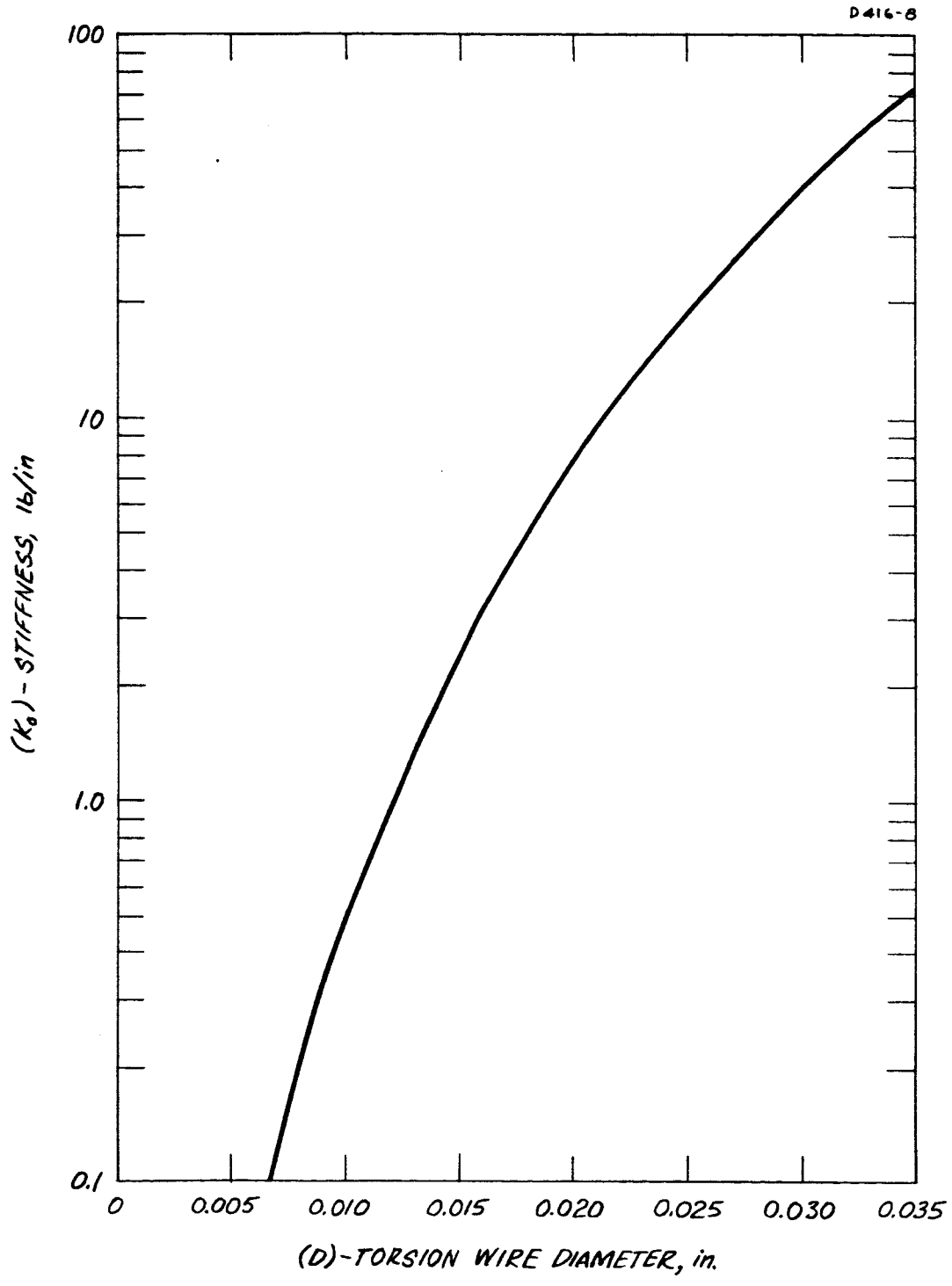

Fig. 11. Torsion wire stiffness.

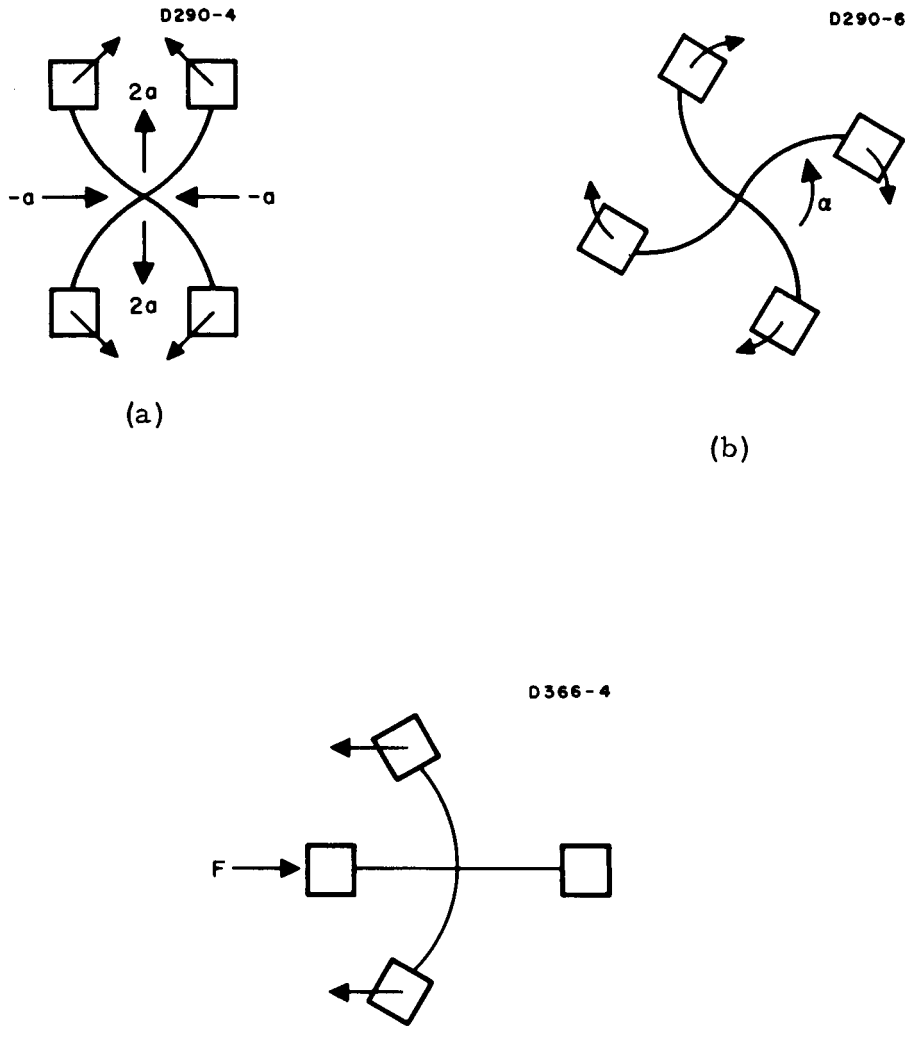

Fig. 12. Sensor vibrational modes.

order modes, as well as the torsional mode, are usually at much higher frequencies than the gradient sensing mode and the two translational modes; they cause relatively little difficulty since they can be easily filtered out.

In our experimental program we have found that it is difficult to design and operate a sensor with a large separation between the various modes. In an effort to develop a better idea of the mode behavior of the cruciform sensor while under rotation, the following analysis was undertaken.

Since we wished to investigate the general behavior of this class of sensors in as rigorous a manner as possible, the model used was not that of one of the actual sensors, but was chosen to be as simple as possible while still retaining many of the important features of the actual sensors. The model (see Fig. 13) assumes a central mass M and four smaller masses m at the ends of four arms of length a; these arms are pivoted at a distance b from the center of the sensor. The sensor was assumed to be in free fall to simplify the analysis.

The kinetic energy of the system is given by the general formula

$$K = \frac{1}{2} M \dot{\vec{R}}^2 + \frac{1}{2} m \sum_{n=1}^{4} \dot{\vec{s}}_n^2 + \frac{1}{2} I \dot{\theta}^2 \qquad (19)$$

where $\vec{R}$ and $\vec{s}$ are shown in Fig. 13, I is the moment of inertia of the central mass M, and $\theta = \Omega + \phi$ is its instantaneous angular velocity. The potential energy of the system is in the springs of the vibrating arms

$$V = \frac{1}{2} k \sum_{n=1}^{4} \alpha_n^2 \qquad (20)$$

where k is the effective spring constant and α_n is the angular deflection of the n^{th} arm. Using these equations, the Lagrangian of the system is therefore

$$L = K - V = \frac{1}{2} M \dot{\vec{R}}^2 + \frac{1}{2} m \sum_{n=1}^{4} \dot{\vec{s}}_n^2 + \frac{1}{2} I \dot{\theta}^2 - \frac{1}{2} k \sum_{n=1}^{4} \alpha_n^2 \, . \qquad (21)$$

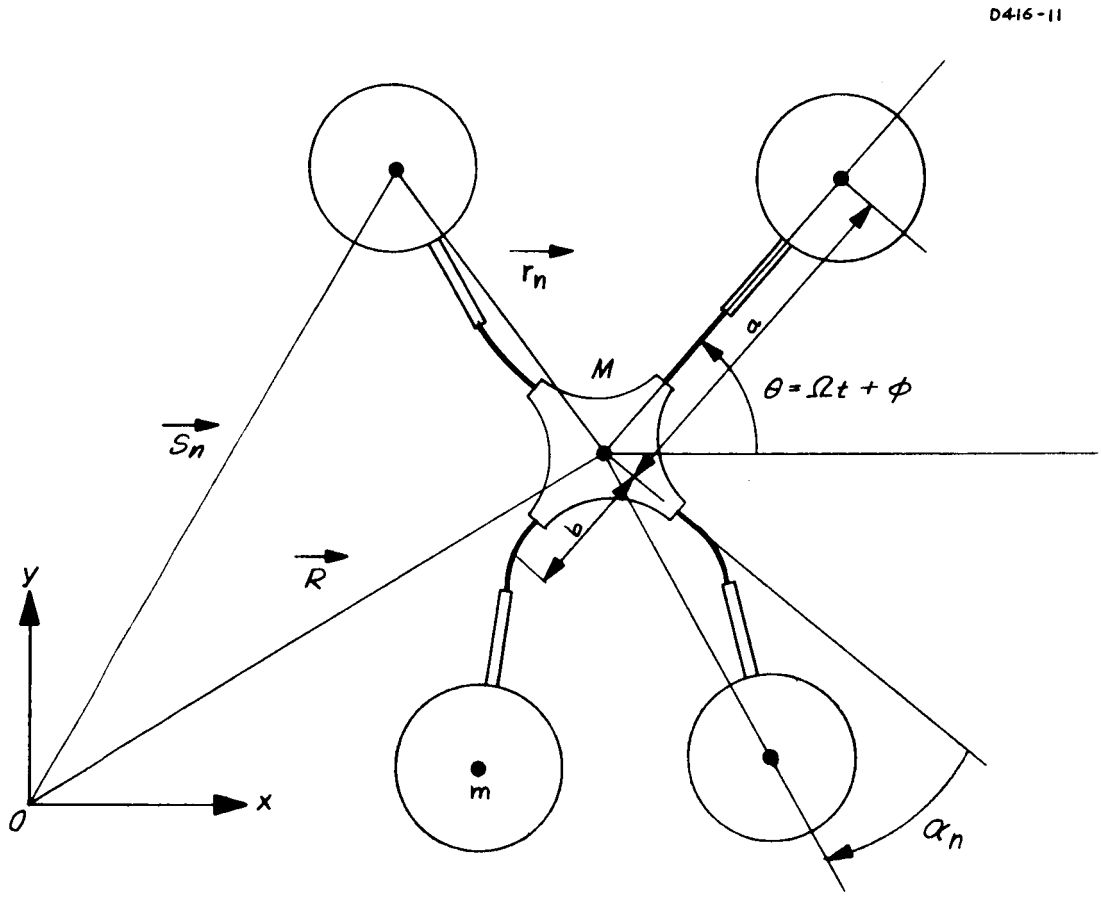

Fig. 13. Model of rotating cruciform sensor.

For our particular system the position of the n^{th} arm is

$$\vec{s}_n = \vec{R} + \vec{r}_n \tag{22}$$

and substituting this into (21) we obtain the Lagrangian in terms of the central mass motion $\dot{\vec{R}}$ and rotation $\dot{\theta}$, and the motion $\dot{\vec{r}}_n$ and position a_n of the arms.

$$L = \frac{1}{2} M\dot{\vec{R}}^2 + \frac{1}{2} m \sum_{n=1}^{4} (\dot{\vec{R}}^2 + 2\dot{\vec{R}} \cdot \dot{\vec{r}}_n + \dot{\vec{r}}_n^2) + \frac{1}{2} I \dot{\theta}^2 - \frac{1}{2} k \sum_{n=1}^{4} a_n^2 . \tag{23}$$

The equation of motion for the central mass is given by

$$- \frac{\partial L}{\partial \vec{R}} + \frac{d}{dt} \frac{\partial L}{\partial \dot{\vec{R}}} = 0 = \frac{d}{dt} \frac{\partial L}{\partial \dot{\vec{R}}} . \tag{24}$$

This gives us an equation expressing the conservation of linear momentum

$$\frac{\partial L}{\partial \dot{\vec{R}}} = \text{constant} = M\dot{\vec{R}} + m\left(4\dot{\vec{R}} + \sum_{n=1}^{4} \dot{\vec{r}}_n\right) . \tag{25}$$

If we assume that the sensor was initially at rest, then $\partial L / \partial \dot{\vec{R}} = 0$ and (25) becomes

$$\dot{\vec{R}} = - \frac{m}{M + 4m} \sum_{n=1}^{4} \dot{\vec{r}}_n . \tag{26}$$

Substituting (26) into (23) and simplifying by combining like terms, we obtain an expression for the Lagrangian in terms of the motion of the arms, and the rotation of the central mass

$$L = \frac{1}{2} m \sum_{n=1}^{4} \dot{\vec{r}}_n^2 - \frac{1}{2} \frac{m^2}{(M + 4m)} \left[\sum_{n=1}^{4} \dot{\vec{r}}_n\right]^2 + \frac{1}{2} I \dot{\theta}^2 - \frac{1}{2} k \sum_{n=1}^{4} a_n^2 . \tag{27}$$

This form of the Lagrangian is still not suitable for our purposes since r_n is a function of the rotation of the sensor θ as well as the angular displacement of the arms a_n relative to the rotating reference frame of the sensor. The position of the arm is given by

$$\vec{r}_n = r_n \left[\vec{l}_x \cos\left(\theta + \frac{n\pi}{2} + a_n\right) + \vec{l}_y \sin\left(\theta + \frac{n\pi}{2} + a_n\right)\right] \quad (28)$$

$$r_n = a\left(1 - \frac{1}{2}\frac{b}{a-b}a_n^2\right) = a - \frac{1}{2}B a_n^2 \quad (29)$$

where $\vec{l}_x$ and $\vec{l}_y$ are unit vectors in the x and y directions respectively, a is the nominal length of the sensor arm, and b is the distance from the effective pivot point to the center of the sensor. B is chosen so that $B = 0$ and $r_n = a$ when the arm is pivoted at the center of rotation ($b = 0$), and B and r_n become indeterminant when the arm is pivoted near the end ($b \approx a$).

The calculation of $\sum_{n=1}^{4} \dot{\vec{r}}_n^2$ and $\left[\sum_{n=1}^{4} \dot{\vec{r}}_n\right]^2$ in terms of θ and a_n is straightforward but tedious and will only be outlined here.

To obtain $\sum_{n=1}^{4} \dot{\vec{r}}_n^2$ we first take the time derivative of (28)

$$\dot{\vec{r}} = \dot{r}_n \left[\vec{l}_x \cos\left(\theta + \frac{n\pi}{2} + a_n\right) + \vec{l}_y \sin\left(\theta + \frac{n\pi}{2} + a_n\right)\right] + r_n \left[-\vec{l}_x \sin\left(\theta + \frac{n\pi}{2} + a_n\right) + \vec{l}_y \cos\left(\theta + \frac{n\pi}{2} + a_n\right)\right](\dot{\theta} + \dot{a}_n) \quad (30)$$

and square it to obtain

$$\dot{\vec{r}}_n^2 = \dot{r}_n^2 + r_n^2 (\dot{\theta} + \dot{a}_n)^2 \quad . \quad (31)$$

Since

$$r_n = a - \frac{1}{2} B \alpha_n^2 \tag{32}$$

$$r_n^2 = a^2 - aB \alpha_n^2 + \frac{1}{4} B^2 \alpha_n^4 \tag{33}$$

$$\dot{r}_n = - B \alpha_n \dot{\alpha}_n \tag{34}$$

$$\dot{r}_n^2 = B^2 \alpha_n^2 \dot{\alpha}_n^2 \quad , \tag{35}$$

we can substitute (33) and (35) into (31) to obtain

$$\dot{\vec{r}}_n^2 = a^2 \dot{\theta}^2 + 2a^2 \dot{\alpha}_n \dot{\theta} + a^2 \dot{\alpha}_n^2 - aB \Omega^2 \alpha_n^2 + \ldots \tag{36}$$

where we have neglected terms of order α_n^3, $\alpha^2 \dot{\phi}$ and higher. When (36) is summed over the four arms we obtain one of the desired terms for substitution into the Lagrangian (27)

$$\sum_{n=1}^{4} \dot{\vec{r}}_n^2 = 4a^2 \dot{\theta}^2 + 2a^2 \dot{\theta} \sum_{n=1}^{4} \dot{\alpha}_n + a^2 \sum_{n=1}^{4} \dot{\alpha}_n^2 - aB \Omega^2 \sum_{n=1}^{4} \alpha_n^2 \, . \tag{37}$$

To obtain a similar expression for

$$\left[\sum_{n=1}^{4} \dot{\vec{r}} \right]^2$$

we first sum over (30)

$$\sum_{n=1}^{4} \dot{\vec{r}}_n = a \sum_{n=1}^{4} (\dot{\theta} + \dot{\alpha}_n) \left[- \vec{1}_x \sin \left(\theta + \frac{n\pi}{2} + \alpha_n \right) + \vec{1}_y \cos \left(\theta + \frac{n\pi}{2} + \alpha_n \right) \right] + \ldots \tag{38}$$

where we have neglected terms of order a_n^2. When this is squared term by term, we obtain a large number of terms either of the form

$$a^2(\dot{\theta} + \dot{a}_1)^2 \tag{39}$$

or

$$2a^2 (\dot{\theta} + \dot{a}_1)(\dot{\theta} + \dot{a}_3) \left[\sin\left(\theta + \frac{\pi}{2} + a_1\right) \sin\left(\theta + \frac{3\pi}{2} + a_3\right) + \cos\left(\theta + \frac{\pi}{2} + a_1\right) \cos\left(\theta + \frac{3\pi}{2} + a_3\right)\right] . \tag{40}$$

(A large number of the products simplify if we remember that $\vec{1}_x \cdot \vec{1}_x = 1$ and $\vec{1}_x \cdot \vec{1}_y = 0$.) The sums of the sine and cosine products can then be expressed as the cosine of the angle differences giving us terms such as

$$\begin{aligned} &2a^2 (\dot{\theta} + \dot{a}_1)(\dot{\theta} + \dot{a}_3) \cos(a_p - a_3 - \pi) \\ &\approx -2a^2 (\dot{\theta} + \dot{a}_1)(\dot{\theta} + \dot{a}_3) \left[1 + \frac{1}{2}(a_1 - a_3)^2\right] \end{aligned} \tag{41}$$

and

$$\begin{aligned} &2a^2 (\dot{\theta} + \dot{a}_1)(\dot{\theta} + \dot{a}_2) \cos\left(a_1 - a_2 - \frac{\pi}{2}\right) \\ &= 2a^2 (\dot{\theta} + \dot{a}_1)(\dot{\theta} + \dot{a}_2) \sin(a_1 - a_2) \\ &\approx 2a^2 (\dot{\theta} + \dot{a}_1)(\dot{\theta} + \dot{a}_2)(a_1 - a_2) \quad . \end{aligned} \tag{42}$$

When all these calculations are carried out and like terms combined (many of them cancelling), we obtain

$$\left[\sum_{n=1}^{4} \dot{\vec{r}}\right]^2 = a^2\left[(\dot{a}_1 - \dot{a}_3)^2 + (\dot{a}_2 - \dot{a}_4)^2\right]$$
$$+ 2a^2\,\Omega\left[(a_1 - a_3)(\dot{a}_2 - \dot{a}_4) - (a_2 - a_4)(\dot{a}_1 - \dot{a}_3)\right]$$
$$+ a^2\Omega^2\left[(a_1 - a_3)^2 + (a_2 - a_4)^2\right] \qquad (43)$$

where we have used $\dot{\theta} = \Omega + \dot{\phi} \approx \Omega$ since $\dot{\phi}$ is of the same order as a. When (43) and (27) are substituted into (27) we obtain the Lagrangian in terms of the arm motions a_n and the central mass rotation θ

$$L = \frac{1}{2} m a^2 \sum_{n=1}^{4} \dot{a}_n^2 + 2m a^2 \dot{\theta}^2 + ma^2 \dot{\theta} \sum_{n=1}^{4} \dot{a}_n$$

$$- \frac{1}{2} \frac{m^2 a^2}{M + 4m} \left\{\left[(\dot{a}_1 - \dot{a}_3)^2 + (\dot{a}_2 - \dot{a}_4)^2\right] + 2\Omega\left[(a_1 - a_3)(\dot{a}_2 - \dot{a}_4)\right.\right.$$
$$\left.\left. - (a_2 - a_4)(\dot{a}_1 - \dot{a}_3)\right] + \Omega^2\left[(a_1 - a_3)^2 + (a_2 - a_4)^2\right]\right\}$$

$$+ \frac{1}{2} I \dot{\theta}^2 - \frac{1}{2}(k + m a B\Omega^2) \sum_{n=1}^{4} a_n^2 \quad . \qquad (44)$$

This form of the Lagrangian contains the description of the behavior of the sensor in terms of the angular displacement a_n of each one of the arms. However, we are interested in the behavior of the vibrational modes of the sensor, so it will simplify things if we express the Lagrangian in terms of the equivalent angular displacement amplitudes of the vibrational modes. Each mode of vibration corresponds to a particular combination of arm amplitudes and phases; the four primary ones are the gradient sensing mode (see Fig. 12(a))

$$a_G = \frac{1}{2}(a_1 - a_2 + a_3 - a_4) \quad , \qquad (45)$$

the torsional mode (see Fig. 12(b))

$$a_T = \frac{1}{2}(a_1 + a_2 + a_3 + a_4) \quad , \tag{46}$$

and the two orthogonal translational modes (see Fig. 12(c))

$$a_+ = \frac{1}{\sqrt{2}}(a_1 - a_3) \tag{47}$$

$$a_- = \frac{1}{\sqrt{2}}(a_2 - a_4) \quad . \tag{48}$$

The two translational modes can also be expressed in terms of right and left handed circulating translational modes which are complex combinations of the orthogonal modes

$$a_R = \frac{1}{\sqrt{2}}(a_+ - ia_-) = \frac{1}{2}(a_1 + ia_2 - a_3 - ia_4) \tag{49}$$

$$a_L = \frac{1}{\sqrt{2}}(a_+ - ia_-) = \frac{1}{2}(a_1 - ia_2 - a_3 + ia_4) \tag{50}$$

where the complex number i indicates a 90° phase lag in the response of the arm vibrating in that particular mode. This second form of the translational modes will be used later in the study of the mode behavior in a rotating system.

It is obvious from inspection that

$$\sum_{n=1}^{4} a_n^2 = a_1^2 + a_2^2 + a_3^2 + a_4^2 = a_G^2 + a_T^2 + a_+^2 + a_-^2$$

$$= a_G^2 + a_T^2 + a_R^2 + a_L^2 \quad , \tag{51}$$

and that

$$\sum_{n=1}^{4} \dot{a}_n = \dot{a}_1 + \dot{a}_2 + \dot{a}_3 + \dot{a}_4 = 2\,\dot{a}_T \quad , \tag{52}$$

so that the Lagrangian (44) in terms of the amplitudes of the normal mode vibrations is given by

$$L = \frac{1}{2} ma^2 (\dot{a}_G^2 + \dot{a}_T^2 + \dot{a}_+^2 + \dot{a}_-^2) + 2ma^2 \dot{\theta}^2 + 2\,ma^2 \dot{\theta}\,\dot{a}_T$$

$$- \frac{m^2 a^2}{M + 4m} \left[\dot{a}_+^2 + \dot{a}_-^2 + 2\Omega\,(a_+ \dot{a}_- - a_- \dot{a}_+) + \Omega^2 (a_+^2 + a_-^2)\right]$$

$$+ \frac{1}{2} I \dot{\theta}^2 - \frac{1}{2} (k + maB\,\Omega^2)(a_G^2 + a_T^2 + a_+^2 + a_-^2) \quad . \tag{53}$$

The equivalent expression using the complex forms of the circulating translational modes is

$$L = \frac{1}{2} ma^2 (\dot{a}_G^2 + \dot{a}_T^2 + 2\,\dot{a}_R \dot{a}_L) + 2ma^2 \dot{\theta}^2 + 2ma^2 \dot{\theta}\,\dot{a}_T$$

$$- \frac{2m^2 a^2}{M + 4m} \left[\dot{a}_R - i\,\Omega\, a_R\right] \left[\dot{a}_L + i\,\Omega\, a_L\right]$$

$$+ \frac{1}{2} I \dot{\theta}^2 - \frac{1}{2} (k + maB\Omega^2)(a_G^2 + a_T^2 + 2\,a_R a_L) \quad . \tag{54}$$

We are now in a position to calculate the equations of motion for the four normal modes.

The equation of motion for the gradient sensing or tuning fork mode (see Fig. 12(b)) is given by

$$\frac{d}{dt} \frac{\partial L}{\partial \dot{a}_G} - \frac{\partial L}{\partial a_G} = 0 \tag{55}$$

or

$$ma^2 \ddot{a}_G + (k + ma\,B\Omega^2)\, a_G = 0 \quad . \tag{56}$$

This harmonic oscillator equation immediately gives us the expression for the frequency of this normal mode

$$\omega_G^2 = \frac{k + ma\,B\Omega^2}{ma^2} = \frac{k + m\left(\frac{ab}{a - b}\right)\Omega}{ma^2} = \frac{k'}{ma^2} \quad . \tag{57}$$

We note here that the frequency of this mode is not constant but shifts upward under rotation. This effect is borne out by the experimental results (see Fig. 5) and is due to the increase in the effective spring constant from the centrifugal force acting on the sensor arms as gravity on a pendulum. However, the centrifugal force does not simulate gravity exactly since it is not a uniform field but extends radially outward. If the pivot point of the arm were at the center of rotation (b = 0), the frequency of the mode would be independent of the rotational speed, since the mass on the end of the arm would not see any variation in the centrifugal potential as the arm vibrated.

The equation of motion for the torsional mode is given by

$$\frac{d}{dt}\frac{\partial L}{\partial \dot{a}_T} - \frac{\partial L}{\partial a_T} = 0 = ma^2 \ddot{a}_T + 2ma^2 \ddot{\theta} + k' a_+ \tag{58}$$

where k' is the effective spring constant under rotation (see eq. 57). The term containing the variation in the central mass rotation speed $\ddot{\theta}$ due to its interaction with the torsional mode is eliminated by the equation

$$\frac{d}{dt}\frac{\partial L}{\partial \dot{\theta}} - \frac{\partial L}{\partial \theta} = 0 = 4ma^2 \ddot{\theta} + 2ma^2 \ddot{a}_T + I\ddot{\theta} \ , \tag{59}$$

or

$$\ddot{\theta} = -\frac{2ma^2}{I + 4ma^2}\ddot{a}_T \quad . \tag{60}$$

Substituting (50) into (58) and combining like terms, we obtain

$$\left(\frac{I\,ma^2}{I + 4ma^2}\right)\ddot{a}_T + k' a_T = 0 \quad . \tag{61}$$

So that the frequency of the torsional vibration normal mode is given by

$$\omega_T^2 = \left(\frac{I + 4\,ma^2}{I\,ma^2}\right) k'$$

$$= \left(\frac{I + 4\,ma^2}{I\,ma^2}\right)\left[k + m\left(\frac{ab}{a-b}\right)\Omega^2\right] = \left(\frac{I + 4\,ma^2}{I\,ma^2}\right)\ \omega_G^2 \ . \tag{62}$$

Here we note that the torsional mode frequency starts off higher than the gradient sensing mode frequency, provided the moment of inertia I of the central mass is not too large, and increases with rotation speed in the same manner. This behavior is borne out by the experimental results. An isolated sensor usually has a sufficiently small central mass that the torsional mode frequency is considerably higher than the gradient sensing mode frequency and rises with increasing rotation speed (see Fig. 5). However, if the sensor is firmly attached to a large sensor chamber, the torsional mode frequency shifts down toward the gradient sensing mode frequency. (See Section II-B in Quarterly Progress Report No. 2.)

The two equations of motion for the two translational modes are given by

$$\frac{d}{dt}\frac{\partial L}{\partial \dot{a}_R} - \frac{\partial L}{\partial a_R} = 0$$

$$= ma^2 \ddot{a}_L - \frac{2m^2 a^2}{M + 4m}\left[\ddot{a}_L + 2i\,\Omega\,\dot{a}_L - \Omega^2 a_L\right] + k' a_L \tag{63}$$

and similarly,

$$\frac{d}{dt}\frac{\partial L}{\partial \dot{a}_L} - \frac{\partial L}{\partial a_L} = 0$$

$$= ma^2 \ddot{a}_R - \frac{2m^2 a^2}{M + 4m}\left[\ddot{a}_R - 2i\,\Omega\,\dot{a}_R - \Omega^2 a_R\right] + k' a_R \ . \tag{64}$$

Letting $a_R = ae^{\pm i\omega t}$ or $a_L = ae^{\mp i\omega t}$, we obtain

$$\omega^2 - \frac{2m}{M + 4m}\left[\omega \pm \Omega\right]^2 - \frac{k'}{ma^2} = 0 \qquad (65)$$

or

$$\left(\frac{M + 2m}{M + 4m}\right)\omega^2 \pm \frac{4m}{M + 4m}\,\Omega\omega - \left(\omega_G^2 + \frac{2m}{M + 4m}\,\Omega^2\right) = 0 \qquad (66)$$

where

$$\omega_G^2 = \frac{k'}{ma^2} = \frac{k + m\left(\frac{ab}{a - b}\right)\Omega^2}{ma^2} \qquad (57)$$

is the square of the resonance frequency of the gradient sensing mode.

Note that if the sensor is not rotating ($\Omega = 0$), the two translational modes have the degenerate frequency

$$\omega^2 = \left(\frac{M + 4m}{M + 2m}\right)\omega_G^2 \quad . \qquad (67)$$

The maximum separation between the translational mode and the gradient sensing mode occurs when the central mass is smaller than the arm mass $M << m$

$$\omega = \sqrt{2}\omega_G = 1.41\ \omega_G \qquad M << m,\ \Omega = 0 \quad . \qquad (68)$$

As the central mass is made larger, the translational frequencies shift downward

$$\omega = \sqrt{\frac{5}{3}}\ \omega_G = 1.29\,\omega_G \qquad M = m,\ \Omega = 0 \qquad (69)$$

until the translational modes are at the same frequency as the gradient sensing mode

$$\omega = \omega_G \qquad M >> m, \ \Omega = 0 \ . \tag{70}$$

This behavior predicted by the theory closely follows our experience during the experimental work.

If the sensor is rotating, the two translational modes split

$$\omega_{\pm} = \left(\frac{M + 4m}{M + 2m}\right) \left[\omega_G^2 + \frac{2m}{M + 4m} \left(\Omega^2 - \omega_G^2\right)\right]^{1/2} (\pm) \frac{2m}{M + 2m} \Omega \ . \tag{71}$$

When the sensor is rotated at $\Omega = \pm\omega_G$, the two translational mode frequencies become

$$\omega_+ = \frac{M + 6m}{M + 2m} \omega_G = \left\{ \begin{array}{rl} 3 \ \omega_G & M << m \\ 2.34 \ \omega_G & M = m \\ \omega_G & M >> m \end{array} \right\} \tag{72}$$

$$\omega_- = \omega_G \tag{73}$$

and we see that the lower of the split translational modes has the same frequency as the gradient sensing mode, independent of the size of the central mass M.

If we assume that the sensor is rotating at its design speed of one-half of the gradient sensing mode frequency ($\Omega = (1/2) \omega_G$), the translational mode frequencies are

$$\omega_{\pm} = \frac{M + 4m}{M + 2m} \left[1 - \frac{3m}{2(M + 4m)}\right]^{1/2} \omega_G \pm \frac{m}{M + 2m} \omega_G \ . \tag{74}$$

For a small central mass $M << m$, the two mode frequencies are

$$\omega_{\pm} = \frac{1}{2} (\sqrt{10} \pm 1) \omega_G \tag{75}$$

or

$$\omega_{+} = 2.081 \, \omega_G \tag{76}$$

$$\omega_{-} = 1.081 \, \omega_G \tag{77}$$

for $M = m$

$$\omega_{+} = 1.728 \, \omega_G \tag{78}$$

$$\omega_{-} = 1.062 \, \omega_G \tag{79}$$

and for a large central mass $M >> m$, we get the expected result (see eq. 70)

$$\omega_{\bullet} = \omega_G \ . \tag{80}$$

This behavior of the two translational modes with rotation speed Ω is plotted in Fig. 14. This curve assumes that the sensor arms are pivoted at the center so that $b = 0$ and there is no increase in the effective spring constant of the arms with increasing rotation speed. An actual curve from the experimental portion of the program is shown in Fig. 15. This sensor has a central mass equal to the mass of one of the arms and the ratio of the measured frequencies at various rotation speeds agree to within 1% of those calculated for $M = m$.

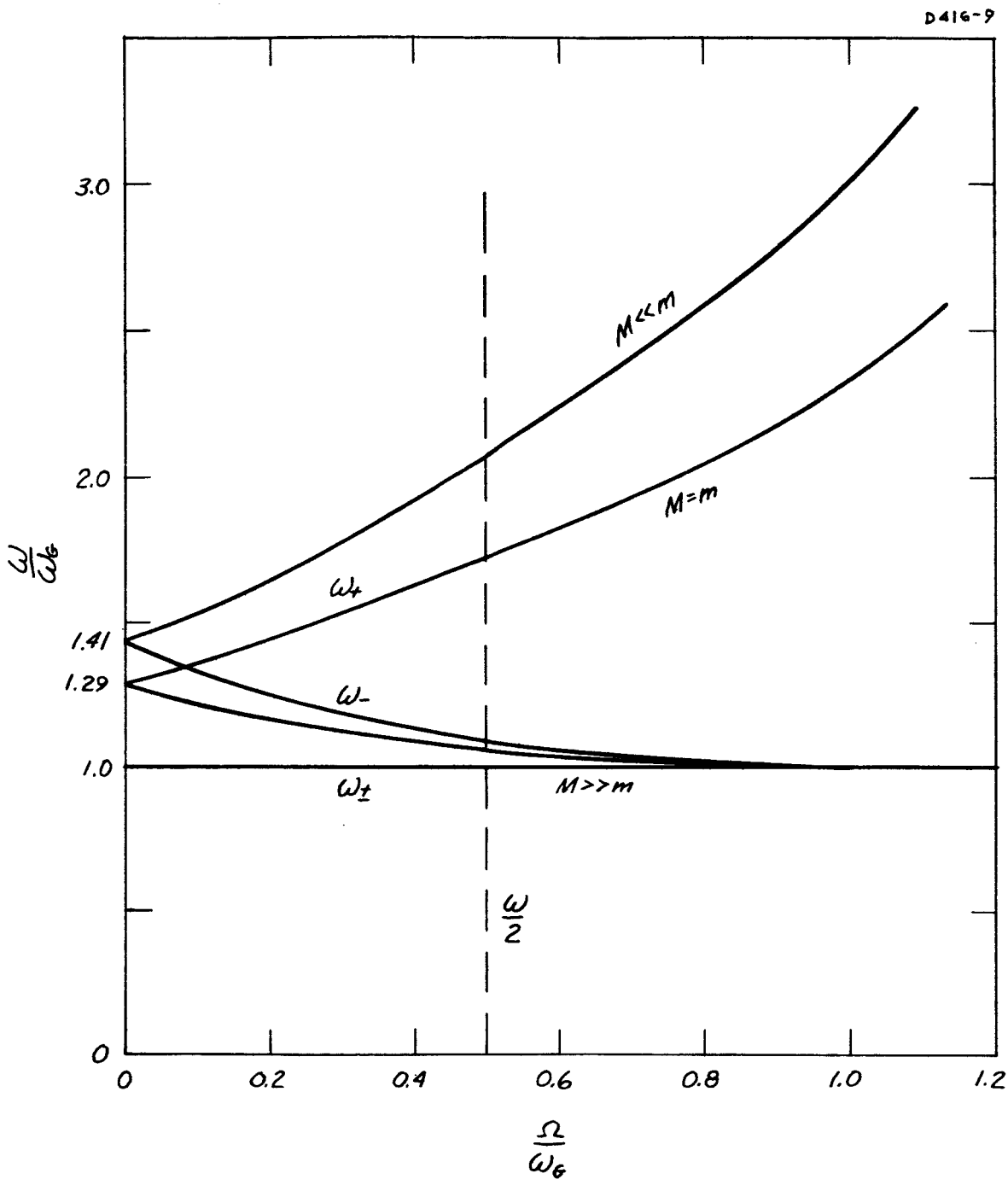

Fig. 14. Predicted translational mode splitting.

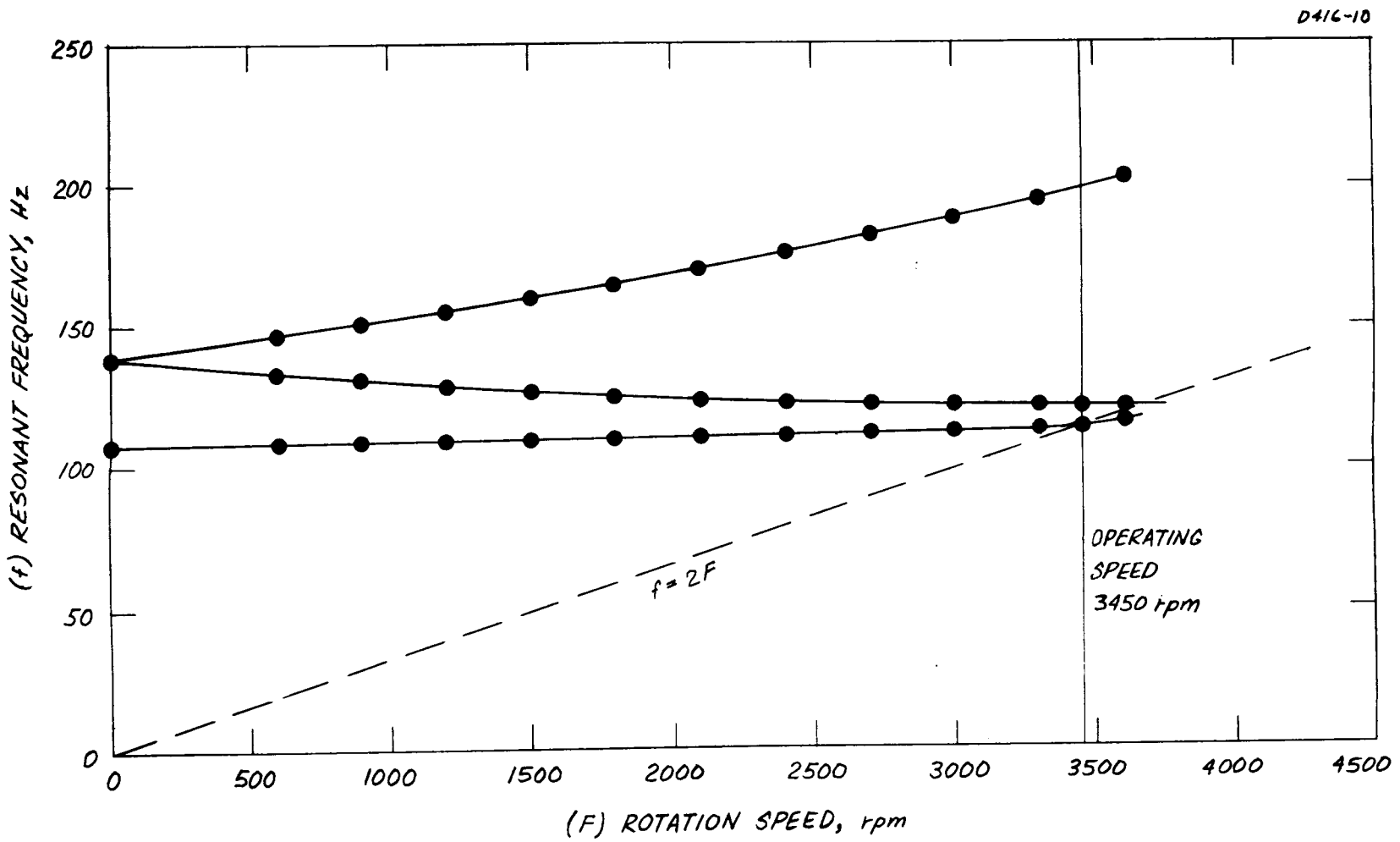

Fig. 15. Measured translational mode splitting.

IV. CONCLUSIONS

The results of the noise tests indicate that our major source of noise at the present time is not caused by air turbulence shaking the sensor vacuum chamber, but by forces induced by slip ring wobble. In addition, because of our inability to obtain a wide mode separation, the present tuned amplifiers do not have a narrow enough bandwidth to completely resolve the various modes and this also leads to large measured noise values. (The new P.A.R. lock-in amplifier, recently purchased from our capital funds to support this project, should eliminate this problem in the future.)

The results of the combined theoretical and experimental work on the behavior of the sensor modes under rotation indicates that it is possible to operate the sensor at the desired rotation speed of one-half of the gradient sensing mode frequency and still maintain adequate frequency separation between the variation sensitive translational modes and the gradient sensing mode. The analysis shows, however, that the maximum frequency separation obtainable will most likely be less than 8%, so that the mechanical Q's of the sensor modes should be relatively high (~100) and the frequency selection techniques should have narrow bandwidths (~1%).

The analysis indicates that a good design for a sensor should have (1) arms with an effective pivot as near the center of rotation as possible so that the frequency shift of the gradient sensing mode is small, and (2) as small a central mass as possible so that there is a maximum amount of separation between modes.

The results of various design studies, presented in this and the previous reports, indicate that our present strain-to-voltage tranducers, amplifiers, and other electronic components are more than adequate for the problem of seeing the gravitational gradient signals.

V. RECOMMENDATIONS

It is recommended that the following investigations be continued:

- Experimental investigation of noise in bearings and drives
- Experimental investigation of sensor mounts
- Theoretical analysis of the cruciform sensor and sensor mount mode behavior under rotation.